IEEE Access
Multidisciplinary | Rapid Review | Open Access Journal

Received January 17, 2022, accepted February 14, 2022, date of publication February 17, 2022, date of current version February 24, 2022.

Digital Object Identifier 10.1109/ACCESS.2022.3152533

Hierarchically Structured Flexible Electrode on Polyimide for Highly Sensitive and Reliable Biosignal Acquisition

JINPYEO JEUNG[1], INYEOL YUN[1], (Student Member, IEEE), YUNSIK KIM[1], SUWON SEONG[1], AND YOONYOUNG CHUNG[1,2], (Member, IEEE)

[1]Department of Electrical Engineering, Pohang University of Science and Technology, Pohang 37673, South Korea
[2]Center for Semiconductor Technology Convergence, Pohang University of Science and Technology, Pohang 37673, South Korea

Corresponding author: Yoonyoung Chung (ychung@postech.ac.kr)

This work was supported in part by the Sports Promotion Fund of Seoul Olympic Sports Promotion Foundation from the Ministry of Culture, Sports, and Tourism, in part by the Educational Institute for Intelligent Information Integration, and in part by the National Research Foundation (NRF) funded by the Ministry of Science and ICT under Grant 2021M3C1C3097512.

ABSTRACT Numerous wearable biomedical devices are developed for the continuous monitoring of personal health or condition. Biosignals acquisition with high sensitivity is important for designing wearable biomedical devices. A sensing electrode between the human body and wearable electronics significantly affects the sensitivity of the sensors. In this study, we fabricated hierarchically structured flexible electrodes on polyimide substrate (HSFE-PI) using micro-casting technique and gold nanoparticles electrodeposition. Polyimides provides robust and outstanding electrical characteristics, and the reliability of HSFE-PI was verified with a cyclic bending test. The integration of hierarchical structures significantly increased the surface area of the electrode by 2.06 times. We applied the HSFE-PI for electromyogram (EMG) and glucose sensing applications and achieved high sensitivity enhancement in both applications. The signal-to-noise ratio (SNR) of measured EMG signals was increased by 2.48 times, and the sensitivity of the glucose detection was increased by 1.42 times compared to the planar counterpart.

INDEX TERMS Flexible electrode, hierarchical structure, biopotential measurement, glucose sensor, wearable sensor, sensitivity enhancement.

I. INTRODUCTION

Wearable biomedical devices have received much attention to monitor individuals' health condition continuously by measuring various biosignals, such as electrocardiogram (ECG), electromyogram (EMG), ion concentration, and blood glucose level, in real time [1]–[6]. In order to design high-performance wearable devices, biosignal acquisitions with high signal-to-noise ratio (SNR) and sufficient sensitivity must be satisfied, as high-quality signals reduce the computational load for signal conditioning and increase the accuracy [7], [8]. A sensing electrode is one of the essential components that affect the sensitivity of biosignal measurements. For example, the electrodes transduce ionic potential inside the human body into an electrical signal or translate the biochemical detection into an electrical signal [9]. Therefore, an optimal design of the sensing electrode is a key to achieve high-quality measurements.

Numerous previous studies on biosignal sensors report that the enlargement of contact area between the sensing electrodes and measured objects leads to a sensitivity enhancement [10]–[12]. For example, the electrodeposition of nanoparticles on biopotential electrodes can increase the surface area, which improves the SNR in ECG and EMG measurements [7]. Similarly, hierarchical structures with micro-/nano- patterns improves the response time and sensitivity of electrochemical sensors through a large surface area [13]–[17]. Thus, a hierarchically structured flexible electrode is an optimal approach to significantly enhance the performance as the hierarchical structures enlarge the surface area, and the flexibility provides a conformal contact with the curvature of the skin.

Polydimethylsiloxane (PDMS) is widely used as a substrate material for the hierarchically structured flexible

The associate editor coordinating the review of this manuscript and approving it for publication was Lorenzo Mucchi.

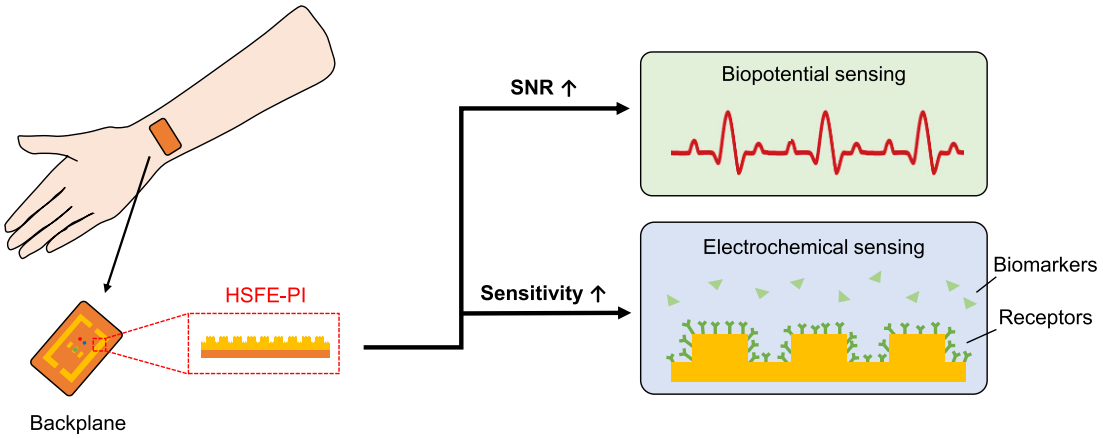

FIGURE 1. Schematic of hierarchically structured flexible electrodes on polyimide substrate (HSFE-PI). HSFE-PI can be utilized in biopotential measurements and an interface for electrochemical sensing. The enlarged surface area in HSFE-PI enhances the signal-to-noise ratio (SNR) and sensitivity.

electrode because of its low cost and facile fabrication [18]. However, a direct deposition of conducting thin film on PDMS is difficult since a large thermal expansion of PDMS induces irreversible cracks on the surface, thereby significantly reducing the reliability and conductivity [19]–[21]. Transfer of conductive materials, such as silver nanowires, gold nanomeshes, carbon nanotubes, and poly(3,4-ethylenedioxythiophene):poly (styrenesulfonate) (PEDOT:PSS) was suggested to avoid the problem [22]. However, the weak adhesion between conductive layer and polymeric substrate makes the fabrication difficult [23]. There were several approaches to form PDMS electrodes by adding carbon-based nanomaterials [24], [25]; however, the nanomaterials suffer from relatively low conductivity [26], which can significantly degrade the signal quality.

In this study, we demonstrated hierarchically structured flexible electrodes on polyimide substrate (HSFE-PI) and applied the electrode to the biosignals measurements (Figure 1). Polyimide (PI), a material conventionally used in microelectronics and flexible displays, was utilized as electrode substrate to provide reliable electrode performance. Despite its excellent characteristics, the use of PI for hierarchically structured flexible electrodes was hindered because most PI patterning approaches, such as dry etching or hot embossing, require high cost and complex process compared to soft lithography [27]. We propose a novel approach to fabricate hierarchical structures using a method combining PI casting process using silicon mold and gold nanoparticles electrodeposition, which reduce the cost and complexity of the fabrication process. The hierarchical structure of HSFE-PI resulted in a considerable increase in the surface area of the electrode. EMG signals were measured and analyzed using HSFE-PI and planar electrodes, and glucose sensors were fabricated by integrating glucose oxidase (GOx) on the electrode. Enhancement in SNR and sensitivity from the hierarchical structure was observed for both applications. The high sensitivity and the stable electrical characteristic of HSFE-PI facilitate the design of reliable and accurate wearable biomedical devices.

II. MATERIALS AND METHODS

A. MATERIALS

Glucose oxidase from Aspergillus niger (GOx, type X-S, 145,200 U/g), glucose, bovine serum albumin (BSA), glutaraldehyde (GLA) solution (25 wt%), potassium ferricyanide(III) ($K_3Fe(CN)_6$), and gold(III) chloride ($HAuCl_4$) solution were purchased from Merck (USA). Sulfuric acid (H_2SO_4, 1 M) was obtained from Samchun (Korea), and a 0.1 M phosphate buffer solution (PBS, pH 7.0) was purchased from Welgene (Korea). All reagents were used without further purification. De-ionized water (18.2 MΩ·cm) was purified with the Millipore Purification System. PI varnish (IPI-N, 5000 cps) was purchased from IPITECH (Korea).

B. PREPARATION OF SILICON MOLD FOR CASTING PROCESS

A positive photoresist (PR) film (2 μm) was spin-coated on a silicon wafer. The PR was patterned into a hole array (100 × 100) using conventional photolithography. Every hole had an identical diameter of 30 μm, and a center-to-center spacing between each hole was 50 μm. The patterned PR was used as a soft mask and the silicon wafer was etched by deep reactive ion etching (DRIE) with a depth of 40 μm. The PR film was removed by sonication in acetone for 5 mins, and the remaining PR residues were further etched by O_2 plasma PR asher. The silicon mold was rinsed with acetone and isopropanol for 5 mins each before use.

C. FABRICATION OF HIERARCHICALLY STRUCTURED FLEXIBLE ELECTRODE ON POLYIMIDE SUBSTRATE (HSFE-PI)

The fabrication process of HSFE-PI is depicted in Figure 2a. The surface of the silicon mold was treated with ultraviolet ozone (UVO) for 20 mins to obtain a hydrophilic surface. A hydrophilic surface decreases the adhesion between PI

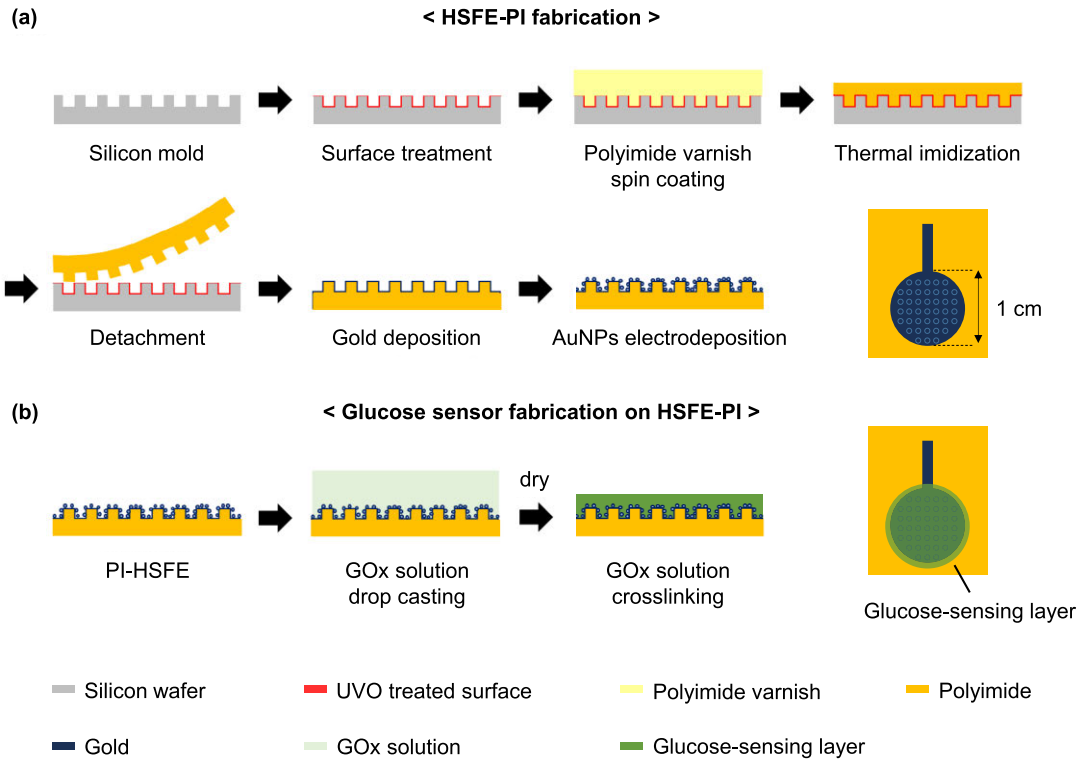

FIGURE 2. Fabrication process of HSFE-PI and glucose sensor. (a) UVO surface treatment facilitates the detachment of PI film from the silicon mold. PI varnish is poured on silicon mold and spin coated. Afterward, PI varnish is thermally imidized to form a micro-structured PI film. The film is detached from the mold, and the gold thin film is deposited on the film by e-beam evaporation. Gold nanoparticles (AuNPs) are electrodeposited on the micro-structured electrode to form hierarchical structures. (b) A glucose sensor is fabricated by immobilizing glucose oxidase (GOx) on HSFE-PI. The immobilization process is performed by crosslinking glutaraldehyde (GLA) and bovine serum albumin (BSA).

and silicon, thus facilitating a detachment of PI from the mold [28]. After the surface treatment, PI varnish was poured on the silicon mold and placed in a vacuum for 210 secs. The vacuum process is required to fully fill the holes with PI varnish. The sample was then spin-coated at 2000 rpm for 60 secs and soft-baked at 200 °C for 5 mins. This coating process was repeated twice to achieve a PI thickness at 10 μm. The sample was hard-baked at 250 °C for 10 mins and 300 °C for 15 mins, for full imidization. Then, the micro-structured PI film was detached from the mold. Titanium (Ti, 5 nm) and gold (Au, 50 nm) were sequentially deposited on the substrate by an e-beam evaporator. A shadow mask was used to define a circular electrode area with a diameter of 10 mm. AuNPs were electrodeposited on the micro-structured gold electrode to complete a hierarchical structures fabrication. Electrodeposition was performed using an electrochemical analyzer (BioLogic SP-200) and a standard three-electrode setup. The three electrodes were composed of an Ag/AgCl reference electrode (1 M KCl), a platinum plate counter electrode, and the micro-structured gold electrode (working electrode). Before an electrodeposition of AuNPs, the surface of the micro-structured Au electrode was electrochemically cleaned by 12 potential cycling between −0.4 to 1.4 V (vs. Ag/AgCl) at a scan rate of 100 mV/s in 50 mM H_2SO_4 until a cyclic voltammetry (CV) output became stable. AuNPs were then electrodeposited on the micro-structured electrode by applying −0.4 V (vs. Ag/AgCl) for 300 secs in a solution containing 5 mM $HAuCl_4$ and 0.5 M KNO_3.

D. FABRICATION OF GLUCOSE SENSOR ON HSFE-PI

Figure 2b illustrates the fabrication process of glucose sensor. GOx was immobilized onto the electrode surface by GLA and BSA crosslinking. Enzyme loading solution (150 μL), which contained 33 μL GLA solution (25%), 7.2 mg BSA, and 30 Units of GOx, was dropped onto the surface of the electrode. The solution was dried at room temperature for 30 mins so that crosslinking of GLA and BSA is progressed. GOx in the loading solution is fixed inside the crosslinked GLA/BSA matrix, thereby forming a glucose-sensing layer. The glucose sensors were stored at 4 °C when not in use to prevent degradation.

E. SEM CHARACTERIZATION OF HSFE-PI

SEM images of HSFE-PI were obtained using a high-resolution FE-SEM (JEOL, JSM-7401F Scanning Electron

Microscope) with an accelerating voltage of 5 kV and working distance of 8 mm.

F. ELECTROCHEMICAL CHARACTERIZATION OF ELECTRODES

CV measurements were performed using a BioLogic SP-200 electrochemical analyzer with a standard three-electrode system described above. For a relative surface area analysis, four types of electrodes were compared: 1) planar gold electrode, 2) AuNPs-deposited gold electrode, 3) micro-structured gold electrode, and 4) HSFE-PI. The planar gold electrode was fabricated by depositing Ti/Au (5/50 nm) on a planar PI substrate (10 μm). With additional AuNPs electrodeposition on the planar gold electrode, AuNPs-deposited gold electrode was obtained. The micro-structured gold electrode was fabricated by deposition of Ti/Au (5/50 nm) thin films on the micro-structured PI substrate. The footprint area of the electrodes was identical (78.5 mm^2). The definition of footprint area and surface area is shown in Figure 3. Utilizing these electrodes as working electrode, 5 CV cycles were performed for each electrode in a 1 M H_2SO_4 solution at a scan rate of 50 mV/s (vs. Ag/AgCl).

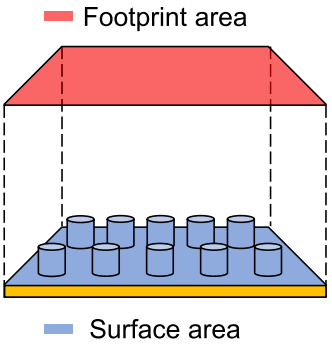

FIGURE 3. Footprint area and surface area in the case of a micro-pillar array. Footprint area indicates a vertically projected area of the micro-pillar array and surface area refers to the area of the part exposed to the exterior.

Electrochemical conduction of electrodes was measured by performing CV in a solution consisting of 5 mM $K_3Fe(CN)_6$ and 1 M KNO_3. The voltage range was from −0.3 to 1.0 V (vs. Ag/AgCl), and the scan rates were varied as follows: 25, 50, 100, 150, and 200 mV/s.

G. EMG SIGNAL ACQUISITION

EMG signal was measured by using a three-lead configuration [7]. A conventional Ag/AgCl electrode was placed on the right wrist of a subject as a reference electrode. The other two electrodes were fixed on the left bicep through skin adhesive with a distance of 5 cm. Two types of electrodes were compared: planar gold electrode and HSFE-PI. An electrolyte gel was applied between the electrodes and the skin. Each electrode was connected to a semiconductor analyzer (Keysight, B1500A) through a BNC cable, and the potential was continuously measured with a sampling rate of 250 Hz while the subject lifted a 2 kg dumbbell continuously.

H. GLUCOSE CONCENTRATION MEASUREMENT

Solutions with various glucose concentrations were prepared by adding glucose to 0.1 M PBS (pH 7.0). CV was performed using a BioLogic SP-200 electrochemical analyzer with the three-electrode system utilizing the glucose sensor as a working electrode (Figure 4). Cyclic voltammograms of the sensors were obtained in different glucose concentrations at a scan rate of 100 mV/s and a voltage range between −0.2 and 0.8 V (vs. Ag/AgCl).

Amperometric measurements of glucose in PBS with the sensor were conducted using the experimental setup described above. The current data was continuously measured by applying a constant potential of 0.8 V (vs. Ag/AgCl). A small amount of highly-concentrated glucose solution (125 mM) was added at an interval of 100 secs to change the glucose concentration from 100 μM to 350 μM. The noise in the measured data was removed by using the Savitzky-Golay filter.

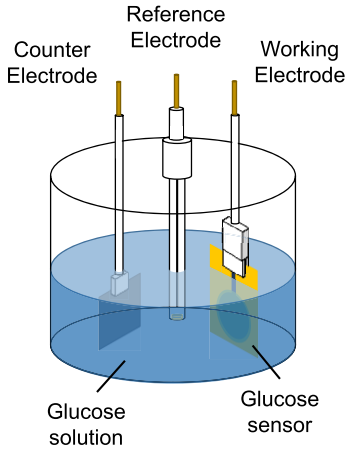

FIGURE 4. Experimental setup for glucose concentration measurements. Ag/AgCl electrode, platinum plate electrode, and glucose sensors were used as a reference, counter, and working electrode, respectively.

III. RESULTS AND DISCUSSION

A. MORPHOLOGY AND SURFACE AREA ENLARGEMENT OF HSFE-PI

Despite its excellent mechanical strength, thermal/chemical stability, and biocompatibility [18], PI was not preferred for hierarchical structure fabrication. This disfavor was due to the difficulties in micro-structuring process of PI. The proposed fabrication approach in this study, combining PI mold casting and AuNPs electrodeposition, produces HSFE-PI with relatively low complexity and fast throughput. The hierarchical structure of HSFE-PI is expected to increase the electrode surface area and electrochemical functionalities.

As shown in Figure 5a, HSFE-PI was successfully fabricated with high yield and fidelity. HSFE-PI is composed of

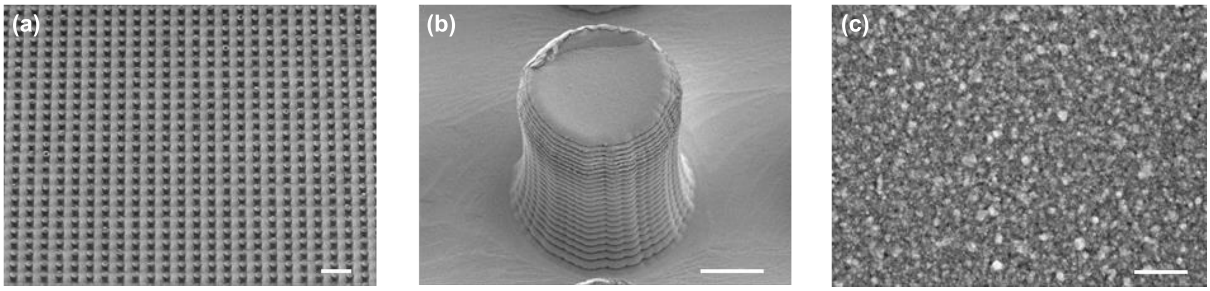

FIGURE 5. SEM images of HSFE-PI. (a) Micro-pillar arrays (100 × 100) are fabricated on PI by casting process using silicon mold. The distance between the centers of each micro-pillar is 50μm. Scale bar: 100μm. (b) Magnified image of single micro-pillar. Diameter and height are approximately 30μm and 40μm, respectively. The scalloped sidewall is originated from the silicon mold fabricated by DRIE process. Scale bar: 10μm. (c) High-magnification image of the electrode surface after electrodeposition. The size of AuNPs is 70–100 nm. Scale bar: 500 nm.

100 × 100 micro-pillars at an interval of 50 μm. Figure 5b shows a magnified SEM image of a single micro-pillar. The diameter and height of the micro-pillar were 30 μm and 40 μm, respectively. As the scallop patterns were formed on the sidewall of silicon mold during the DRIE process, the side of the micro-pillar also contains scallops. The electrodeposited AuNPs with a size of 70-100 nm were observed on the surface of micro-pillars at higher magnification (Figure 5c). AuNPs increased the roughness of electrode surface thereby significantly enlarging the surface area.

In order to study the surface area increment in each method, four types of electrodes were compared: planar gold electrode, AuNPs-deposited gold electrode, micro-structured gold electrode, and HSFE-PI (Figure 6a). The footprint area of all the electrodes was identical to be 78.5 mm^2. Figure 6b shows the cyclic voltammogram of the electrodes in 1 M H_2SO_4 solution. The cyclic voltammograms which is consistent with previous studies [29], [30], exhibit a reduction peak of gold oxide near 0.9 V. As the enlargement of contact area between gold and solution increases a reduction current, the larger reduction peak indicates the increased surface area. For quantitative analysis on the surface area, the charge involved in gold reduction was calculated for each electrode by integrating the area under the reduction peak [13]. The relative surface area of the electrodes was calculated by comparing the calculated charge. The relative surface area is summarized in Table 1.

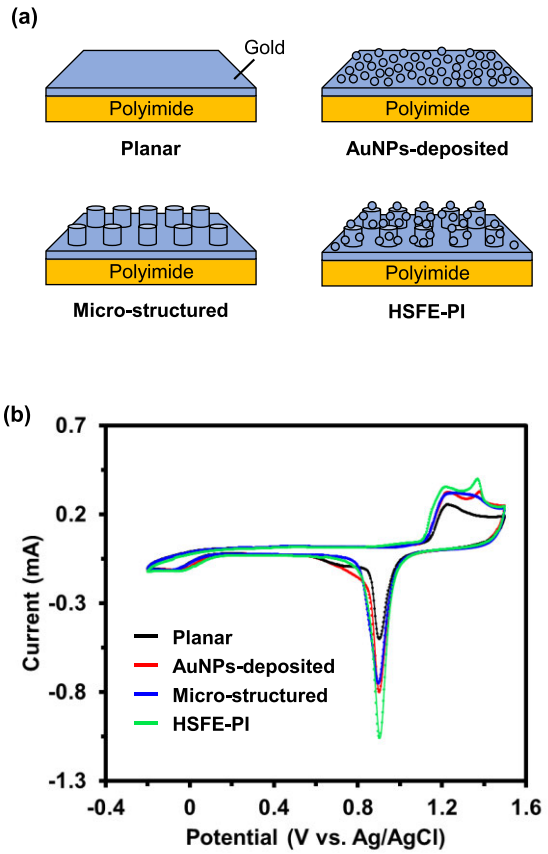

FIGURE 6. Relative surface area comparison between planar gold electrode, AuNPs-deposited gold electrode, micro-structured gold electrode, and HSFE-PI. (a) Structure of 4 electrodes used in this study. (b) Cyclic voltammograms of 4 electrodes in a 1 M H_2 SO_4 solution (scan rate: 50 mV/s). The reduction peak was observed at 0.9 V for all electrodes. As the charge transferred during gold reduction is proportional to electrode surface area, the charge was quantified by integrating the graph area in the reduction state.

TABLE 1. Relative surface area of planar, AuNPs-deposited, micro-structured gold electrodes, and HSFE-PI. The footprint area of each electrode is identical: 78.5 mm^2.

Electrode Type	Relative Surface Area
Planar	1
AuNPs-deposited	1.56
Micro-structured	1.49
HSFE-PI	2.06

Theoretical surface area increment by micro-structures can be calculated by equation (1) [33], assuming the micro-pillar as an ideal cylinder.

$$\frac{S_f + L \cdot h}{S_f} = 1 + \frac{(\pi \cdot d \cdot N) \cdot h}{S_f}, \quad (1)$$

where S_f is the footprint area of the electrode, L is the contour length, h is the height of cylinder, d is the diameter of cylinder, and N is the number of cylinders. As S_f is 78.5 mm^2, d is 30 μm, N is 10^4, and h is 40 μm, the theoretical surface area increment is 1.48. The measured surface area of the micro-structured electrode was 1.49 times larger than the planar electrode, which is almost identical to the theoretical estimation. The electrodeposition of AuNPs on the planar gold electrode increased the surface area by 1.56 times. Hierarchical structures significantly enlarged the surface area, which was verified by a 2.06 times larger surface area of HSFE-PI compared to the planar electrode. Furthermore, HSFE-PI exhibits superior surface area enhancement compared to the previous studies on skin-electrode (Table 2).

TABLE 2. Comparison of surface area enlargement with previous skin-electrode studies.

Reference	Enlargement Method	Surface Area Enlargement
[31]	Pyramid array micro-structure	1.18
[7]	AuNPs deposition	1.54
[32]	Micro-pillar array structure	1.61
This work	HSFE-PI	2.06

B. ELECTROCHEMICAL CHARACTERIZATION OF HSFE-PI

The transduction efficiency of electrochemical signals was evaluated for the planar gold electrode and HSFE-PI. Figure 7a exhibits the CV response using solution containing 5 mM $K_3Fe(CN)_6$ and 1 M KNO_3 at a scan rate of 200 mV/s. HSFE-PI shows substantially higher peak current compared to the planar electrode in the $Fe(CN)_6^{4-/3-}$ redox environment. The anodic peak current (I_p) of HSFE-PI and planar electrode was measured to be 1.99 mA and 1.09 mA, respectively. The electrochemically active surface area (ECSA) of the electrodes was determined using the Randles-Sevcik equation [34]:

$$I_p = 2.69 \times 10^5 \cdot n^{\frac{3}{2}} \cdot A \cdot D^{\frac{1}{2}} \cdot C \cdot \nu^{\frac{1}{2}}, \quad (2)$$

where n is the number of electrons transferred in the redox event, A is the ECSA of the electrode (cm^2), D is the diffusion coefficient of the analyte in bulk solution (cm^2/s), C is the concentration of the analyte (mol/cm^3), and ν is the scan rate (V/s). As the $Fe(CN)_6$ redox environment is a representative system that exhibits a heterogeneous one-electron transfer, n equals 1 [35]. The diffusion coefficient of $Fe(CN)_6^{3-}$ in solution consisted of 5 mM $K_3Fe(CN)_6$ and 1 M KNO_3 is 5.0×10^{-6} cm^2/s [34]. The ECSA of the planar electrode was 80 mm^2, which is almost identical to the footprint area of 78.5 mm^2. The ECSA of HSFE-PI was extracted to be 147 mm^2, which was 1.86 times larger than its footprint area. As shown in Figure 7b, the peak currents have a linear relationship with the square root of the scan rate. This result suggests that the electrochemical reaction of $Fe(CN)_6^{3-/4-}$ on the surface of the electrode was a diffusion-controlled process [36]. Thus, the use of HSFE-PI can bring substantial enhancement of sensitivity to electrochemical sensors.

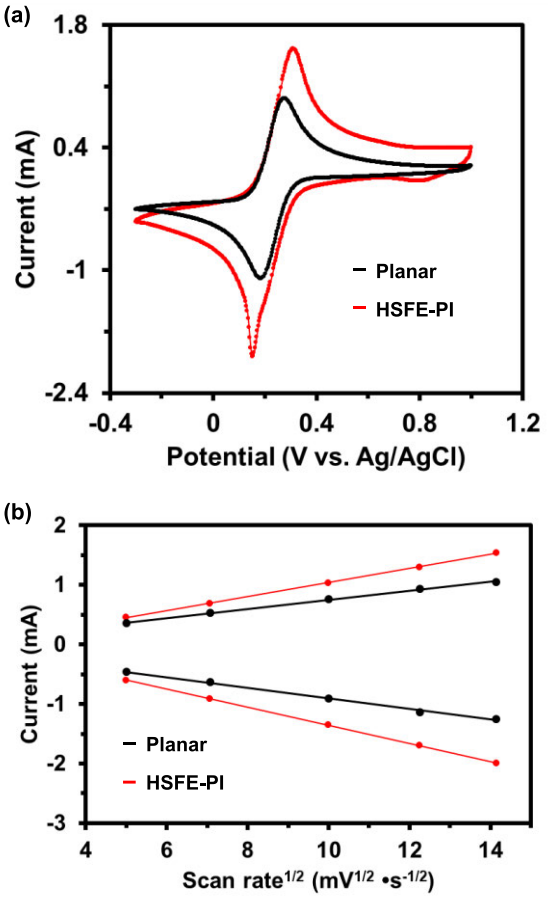

FIGURE 7. Electrochemical characterization of planar gold electrode and HSFE-PI. (a) Cyclic voltammogram of both electrodes using solution containing 5 mM K_3 $Fe(CN)_6$ and 1 M KNO_3 at a 200 mV/s scan rate. The anodic peak currents for the planar electrode and HSFE-PI were 1.09 and 1.99 mA, respectively. The cathodic peak currents for planar and HSFE-PI were 0.97 and 1.54 mA, respectively. The larger peak current indicates the larger electrochemically active surface area (ECSA) of HSFE-PI. (b) Peak current data as a function of the square root of scan rate. Linear relationship between peak current and square root of scan rate indicates that redox reaction is a diffusion-controlled process.

C. MECHANICAL STABILITY OF HSFE-PI

As most wearable devices are used in various non-planar conditions, the reliability of flexible electrodes is an important parameter. A cyclic bending test was performed to confirm the reliability of HSFE-PI (Figure 8). HSFE-PI was repeatedly bent for 10,000 cycles with a bending radius of 5 mm using R-bending system (Sciencetown, Korea). The sheet resistance of HSFE-PI was measured by the 4-point probe method in every 2,000 cycles using setup described in [37]. HSFE-PI exhibited stable sheet resistance throughout the cyclic bending test, which implies that HSFE-PI can retain its outstanding electrical performance while forming a conformal contact with the skin.

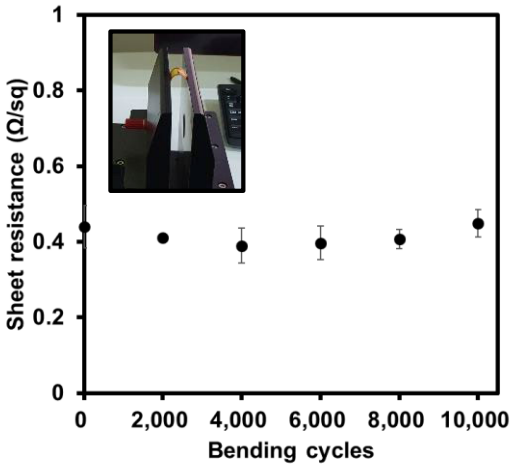

FIGURE 8. Sheet resistance of HSFE-PI during cyclic bending test with a bending radius of 5 mm. Inset shows experimental setup for the cyclic bending test. HSFE-PI exhibits stable sheet resistance at 10,000 cycles.

D. EMG MEASUREMENTS

EMG signals were measured on the biceps using planar electrodes and HSFE-PIs (Figure 9a). Two signal electrodes were placed on the left bicep with a 5 cm distance, as shown in Figure 9b, and a conventional Ag/AgCl electrode was placed on the right wrist as a reference. As the electrode substrate was thin and flexible, they formed a conformal contact with curvilinear human skin. Figure 9c shows EMG signals measured by the planar electrodes and HSFE-PIs. The amplitude of EMG signal measured by HSFE-PI is much larger than the planar electrode due to the larger surface area, which leads to the lower contact resistance. To calculate the SNR of EMG, the signal during muscle contraction (S_S) and the noise signal without any muscle contraction (S_n) were measured for the same time period. Then, the SNR was calculated by equation (3) [38].

$$\mathrm{SNR} = 20 \cdot \log_{10} \sqrt{\frac{\sum S_S^2}{\sum S_n^2}}, \tag{3}$$

The SNR of planar electrode and HSFE-PI were 5.1 and 12.7, respectively. The HSFE-PI exhibited 2.5 times higher SNR compared to the planar electrode. Comparison of our HSFE-PI electrode with previously reported skin electrodes is summarized in Table 3. The SNR values were normalized by area for a fair comparison, and our HSFE-PI exhibits high sensitivity.

E. GLUCOSE SENSOR CHARACTERIZATION

The glucose sensor was fabricated by immobilizing GOx on the surface of electrodes through GLA/BSA crosslinking method. The detailed glucose sensing mechanism is described by the following equations [41]:

$$\mathrm{Glucose} + \mathrm{GOx(FAD)} \rightarrow \mathrm{Gluconic\ acid} + \mathrm{GOx(FADH)} \tag{4}$$

$$\mathrm{GOx(FADH_2)} + \mathrm{O_2} \rightarrow \mathrm{GOx(FAD)}{+}\mathrm{H_2O_2} \tag{5}$$

$$\mathrm{H_2O_2} \rightarrow 2\mathrm{H^+} + \mathrm{O_2} + 2\mathrm{e^-} \tag{6}$$

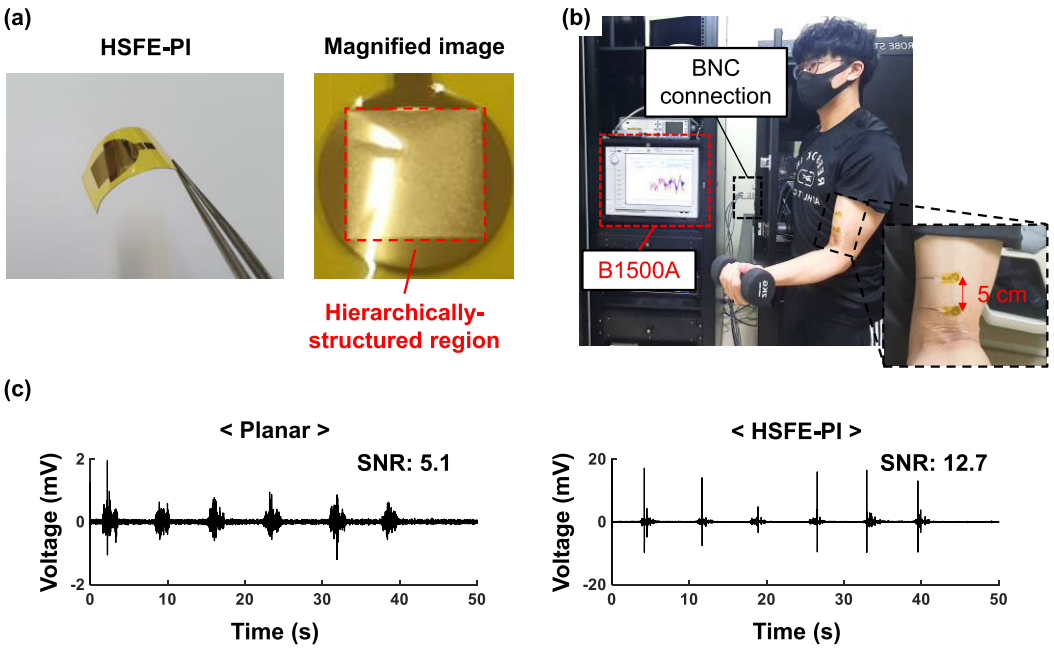

FIGURE 9. EMG signal acquisition using planar electrode and HSFE-PI. (a) Photographs of HSFE-PI. HSFE-PI exhibits excellent flexibility, providing conformal contact with the skin. (b) Experimental setup for EMG signal acquisition. (c) Measured EMG signal using the electrodes. Amplitude of the acquired EMG signal using HSFE-PI was larger than the planar gold electrode, which resulted in higher SNR. SNR of the EMG signal for the planar electrode and HSFE-PI was 5.1 and 12.7, respectively.

TABLE 3. Performances comparison with previously reported skin electrodes.

Reference	Electrode	Footprint area (cm^2)	Normalized SNR [a.u.]
[39]	Woven textile electrode	7.50	2.85
[40]	MWCNTs/PDMS composite on Silver	7.07	3.27
[24]	CNT/PDMS composite electrode	12.56	3.65
[38]	PEDOT:PSS electrode	0.79	13.94
This work	HSFE-PI	0.79	16.17

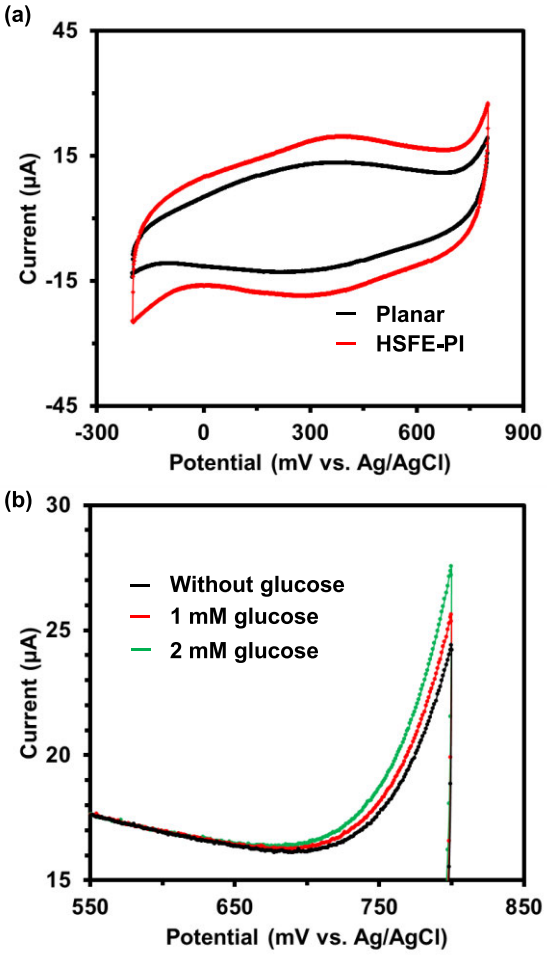

FIGURE 10. Electrochemical characterization of the glucose sensors. (a) Cyclic voltammogram of glucose sensors fabricated on planar gold electrode and HSFE-PI with 2 mM glucose in PBS. (b) Cyclic voltammogram of HSFE-PI glucose sensor under various glucose concentrations. The output current increases as the glucose concentration increases.

Immobilized GOx converts glucose into gluconic acid and produces H_2O_2 (3 and 4). When the produced H_2O_2 diffuses to the electrode surface, it is oxidized, and an electron transfer occurs (5), which generates current. Cyclic voltammograms of glucose sensors fabricated on the planar gold electrode and HSFE-PI were measured in a solution of 2 mM glucose in PBS (Figure 10a). The HSFE-PI glucose sensor shows a higher current level than that of the planar electrode, which implies higher electrochemical sensitivity. The anodic peak current of the HSFE-PI glucose sensor was 1.42 times higher compared to the planar electrode sensor. The higher sensitivity achieved by HSFE-PI is attributed to its large ECSA as it facilitates an oxidation of the H_2O_2. As shown in Figure 10b, HSFE-PI glucose sensor can distinguish different glucose concentrations.

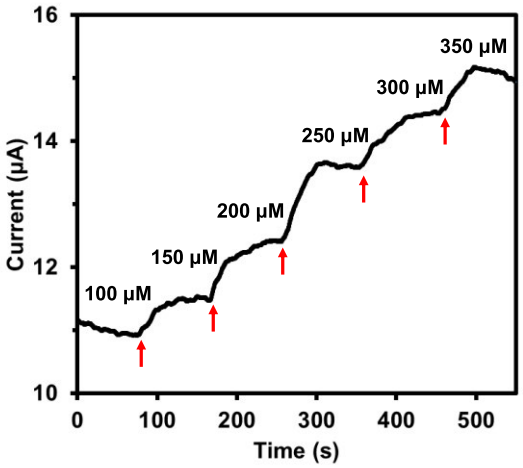

FIGURE 11. Amperometric response of HSFE-PI glucose sensor with periodic additions of concentrated glucose solution. Numbers in the graph represent the corresponding glucose concentration in the measured solution. Arrows indicate the time when the highly-concentrated glucose solution was added.

Figure 11 shows an amperometric response of the HSFE-PI glucose sensor. The output current was increased as glucose was repeatedly added. The sensitivity of the sensor was calculated by using a two-point method [42], [43], and it was 18.9 $\mu A \cdot mM^{-1} \cdot cm^{-2}$. Comparison of our HSFE-PI glucose sensors with previous studies is summarized in Table 4. Our HSFE-PI glucose sensor exhibits high sensitivity with excellent flexibility, which demonstrates the potential of HSFE-PI to the wearable electrochemical sensors.

TABLE 4. Glucose sensor sensitivity comparison with previous studies.

Reference	Electrode	Sensitivity ($\mu A \cdot mM^{-1} \cdot cm^{-2}$)	Flexibility
[44]	GOx-Au/Polystyrene	1.76	O
[45]	GOx-GLA-CA/NPG	3.53	X
[46]	GOx/NPG/GCE	12.1	X
[47]	GOx-PPG-PB/Carbon /PET	12.69	O
[48]	NiO QDs-ZnO NRs/PI	13.14	O
This work	GOx/HSFE-PI	18.9	O

(Cys)-cysteine, (CA)-cysteamine, (NPG)-nanoporous gold, (PPG)- poly (N-phenylglycine), (PB)-prussian blue, (QDs)-quantum dots

IV. CONCLUSION

In this study, HSFE-PI was fabricated by electrodeposition of AuNPs on a micro-structured electrode. The micro-structured electrode was prepared by the PI mold casting process. HSFE-PI exhibited a high surface area, which was 2.06 times larger than the planar electrode. Also, the reliability of HSFE-PI was confirmed by the cyclic bending test. The effects of hierarchical structures were confirmed by both biopotential and electrochemical measurements. The hierarchical structures increased the SNR of EMG by 2.5 times and the sensitivity of the glucose sensor by 1.42 times. The fabricated HSFE-PI glucose sensor exhibited high sensitivity and flexibility. Therefore, HSFE-PI is suitable for the next-generation wearable biomedical applications.

REFERENCES

[1] A. T. Satti, J. Park, J. Park, H. Kim, and S. Cho, "Fabrication of parylene-coated microneedle array electrode for wearable ECG device," *Sensors*, vol. 20, no. 18, p. 5183, Sep. 2020.
[2] W. Sato, K. Murata, Y. Uraoka, K. Shibata, S. Yoshikawa, and M. Furuta, "Emotional valence sensing using a wearable facial EMG device," *Sci. Rep.*, vol. 11, no. 1, Mar. 2021.
[3] H. Y. Y. Nyein, L. C. Tai, Q. P. Ngo, M. Chao, G. B. Zhang, W. Gao, M. Bariya, J. Bullock, H. Kim, H. M. Fahad, and A. Javey, "A wearable microfluidic sensing patch for dynamic sweat secretion analysis," *ACS Sensors*, vol. 3, no. 5, pp. 944–952, May 2018.
[4] I. Yun, J. Jeung, Y. Song, and Y. Chung, "Non-invasive quantitative muscle fatigue estimation based on correlation between sEMG signal and muscle mass," *IEEE Access*, vol. 8, pp. 191751–191757, 2020.
[5] Y. Yao, J. Chen, Y. Guo, T. Lv, Z. Chen, N. Li, S. Cao, B. Chen, and T. Chen, "Integration of interstitial fluid extraction and glucose detection in one device for wearable non-invasive blood glucose sensors," *Biosensors Bioelectron.*, vol. 179, May 2021, Art. no. 113078.
[6] I. Yun, J. Jeung, M. Kim, Y.-S. Kim, and Y. Chung, "Ultra-low power wearable infant sleep position sensor," *Sensors*, vol. 20, no. 1, p. 61, Dec. 2019.
[7] I. Yun, J. Jeung, H. Lim, J. Kang, S. Lee, S. Park, S. Seong, S. Park, K. Cho, and Y. Chung, "Stable bioelectric signal acquisition using an enlarged surface-area flexible skin electrode," *ACS Appl. Electron. Mater.*, vol. 3, no. 4, pp. 1842–1851, Apr. 2021.
[8] I. Yun, J. Jeung, and Y. Chung, "Quantitative muscle fatigue estimation with high SNR flexible skin electrode," in *Proc. 42nd Annu. Int. Conf. IEEE Eng. Med. Biol. Soc. (EMBC)*, Montreal, QC, Canada, Jul. 2020, pp. 4134–4137.
[9] J. Kim, A. S. Campbell, B. E.-F. de Ávila, and J. Wang, "Wearable biosensors for healthcare monitoring," *Nature Biotechnol.*, vol. 37, no. 4, pp. 389–406, Apr. 2019.
[10] H.-L. Peng, J.-Q. Liu, H.-C. Tian, B. Xu, Y.-Z. Dong, B. Yang, X. Chen, and C.-S. Yang, "Flexible dry electrode based on carbon nanotube/polymer hybrid micropillars for biopotential recording," *Sens. Actuators A, Phys.*, vol. 235, no. 1, pp. 48–56, Nov. 2015.
[11] M. A. Yokus and J. S. Jur, "Fabric-based wearable dry electrodes for body surface biopotential recording," *IEEE Trans. Biomed. Eng.*, vol. 63, no. 2, pp. 423–430, Feb. 2016.
[12] E. Castagnola, L. Maiolo, E. Maggiolini, A. Minotti, M. Marrani, F. Maita, A. Pecora, G. N. Angotzi, A. Ansaldo, M. Boffini, L. Fadiga, G. Fortunato, and D. Ricci, "PEDOT-CNT-Coated low-impedance, ultra-flexible, and brain-conformable micro-ECoG arrays," *IEEE Trans. Neural Syst. Rehabil. Eng.*, vol. 23, no. 3, pp. 342–350, May 2015.
[13] C. M. Gabardo, Y. Zhu, L. Soleymani, and J. M. Moran-Mirabal, "Bench-top fabrication of hierarchically structured high-surface-area electrodes," *Adv. Funct. Mater.*, vol. 23, no. 24, pp. 3030–3039, Jun. 2013.
[14] X. Lu, Y. Xiao, Z. Lei, and J. Chen, "Graphitized macroporous carbon microarray with hierarchical mesopores as host for the fabrication of electrochemical biosensor," *Biosensors Bioelectron.*, vol. 25, no. 1, pp. 244–247, Sep. 2009.
[15] Z. Wen, S. Ci, and J. Li, "Pt nanoparticles inserting in carbon nanotube arrays: Nanocomposites for glucose biosensors," *J. Phys. Chem. C*, vol. 113, no. 31, pp. 13482–13487, Aug. 2009.
[16] L. Soleymani, Z. Fang, E. H. Sargent, and S. O. Kelley, "Programming the detection limits of biosensors through controlled nanostructuring," *Nature Nanotechnol.*, vol. 4, no. 12, pp. 844–848, Dec. 2009.
[17] L. Soleymani, Z. Fang, B. Lam, X. Bin, E. Vasilyeva, A. J. Ross, E. H. Sargent, and S. O. Kelley, "Hierarchical nanotextured microelectrodes overcome the molecular transport barrier to achieve rapid, direct bacterial detection," *ACS Nano*, vol. 5, no. 4, pp. 3360–3366, Apr. 2011.
[18] B. J. Kim and E. Meng, "Review of polymer MEMS micromachining," *J. Micromech. Microeng.*, vol. 26, no. 1, Jan. 2016, Art. no. 013001.
[19] R. Seghir and S. Arscott, "Controlled mud-crack patterning and self-organized cracking of polydimethylsiloxane elastomer surfaces," *Sci. Rep.*, vol. 5, no. 1, pp. 1–16, Oct. 2015.
[20] N. Chou, J. Jeong, and S. Kim, "Crack-free and reliable lithographical patterning methods on PDMS substrate," *J. Micromech. Microeng.*, vol. 23, no. 12, Dec. 2013, Art. no. 125035.
[21] N. Chou, S. Yoo, and S. Kim, "Fabrication of stretchable and flexible electrodes based on PDMS substrate," in *Proc. IEEE 25th Int. Conf. Micro Electro Mech. Syst. (MEMS)*, Paris, France, Jan. 2012, pp. 247–250.
[22] G. Li, Z. Qiu, Y. Wang, Y. Hong, Y. Wan, J. Zhang, J. Yang, Z. Wu, W. Hong, and C. F. Guo, "PEDOT: PSS/grafted-PDMS electrodes for fully organic and intrinsically stretchable skin-like electronics," *ACS Appl. Mater. Interfaces*, vol. 11, no. 10, pp. 10373–10379, Mar. 2019.
[23] N. Chou, Y. Kim, and S. Kim, "A method to pattern silver nanowires directly on wafer-scale PDMS substrate and its applications," *ACS Appl. Mater. Interfaces*, vol. 8, no. 9, pp. 6269–6276, Mar. 2016.
[24] H.-C. Jung, J.-H. Moon, D.-H. Baek, J.-H. Lee, Y.-Y. Choi, J.-S. Hong, and S.-H. Lee, "CNT/PDMS composite flexible dry electrodes for long-term ECG monitoring," *IEEE Trans. Biomed. Eng.*, vol. 59, no. 5, pp. 1472–1479, May 2012.
[25] J. H. Lee, Y. W. Nam, H.-C. Jung, D.-H. Baek, S.-H. Lee, and J. S. Hong, "Shear induced CNT/PDMS conducting thin film for electrode cardiogram (ECG) electrode," *BioChip J.*, vol. 6, no. 1, pp. 91–98, Mar. 2012.
[26] X. Hu, Y. Dou, J. Li, and Z. Liu, "Buckled structures: Fabrication and applications in wearable electronics," *Small*, vol. 15, no. 32, Aug. 2019, Art. no. 1804805.
[27] O. Sahin, M. Ashokkumar, and P. M. Ajayan, "Micro- and nanopatterning of biomaterial surfaces," in *Fundamental Biomaterials: Metals*. Amsterdam, The Netherlands: Elsevier, 2018, pp. 67–78.
[28] H.-S. Jeong, R. C. White, Y. Z. Chu, and C. J. During, "Adhesion study of polyimide to Si surfaces," *Surf. Interface Anal.*, vol. 18, no. 4, pp. 289–292, Apr. 1992.
[29] C. Jeyabharathi, U. Hasse, P. Ahrens, and F. Scholz, "Oxygen electroreduction on polycrystalline gold electrodes and on gold nanoparticle-modified glassy carbon electrodes," *J. Solid State Electrochem.*, vol. 18, no. 12, pp. 3299–3306, Dec. 2014.
[30] X. Gu, X. Li, S. Wu, J. Shi, G. Jiang, G. Jiang, and S. Tian, "A sensitive hydrazine hydrate sensor based on a mercaptomethyl-terminated trinuclear Ni(ii) complex modified gold electrode," *RSC Adv.*, vol. 6, no. 10, pp. 8070–8078, 2016.
[31] S. Wang, J. Yan, C. Zhu, J. Yao, Q. Liu, and X. Yang, "A low contact impedance medical flexible electrode based on a pyramid array microstructure," *Micromachines*, vol. 11, no. 1, p. 57, Jan. 2020.
[32] S. Kaitainen, A. Kutvonen, M. Suvanto, T. T. Pakkanen, R. Lappalainen, and S. Myllymaa, "Liquid silicone rubber (LSR)-based dry bioelectrodes: The effect of surface micropillar structuring and silver coating on contact impedance," *Sens. Actuators A, Phys.*, vol. 206, pp. 22–29, Feb. 2014.
[33] J. Shieh, C. You, C. Chiu, J. Liu, and P. Shih, "Black-silicon on micropillars with minimal surface area enlargement to enhance the performance of silicon solar cells," *Nanosc. Res. Lett.*, vol. 11, no. 1, pp. 1–7, Nov. 2016.
[34] Z. O. Ameur and M. M. Husein, "Electrochemical behavior of potassium ferricyanide in aqueous and (w/o) microemulsion systems in the presence of dispersed nickel nanoparticles," *Separat. Sci. Technol.*, vol. 48, no. 5, pp. 681–689, Jan. 2013.
[35] Z. Zhu, W. Song, K. Burugapalli, F. Moussy, Y.-L. Li, and X.-H. Zhong, "Nano-yarn carbon nanotube fiber based enzymatic glucose biosensor," *Nanotechnology*, vol. 21, no. 16, Apr. 2010, Art. no. 165501.
[36] V. Augustyn, J. Come, M. A. Lowe, J. W. Kim, P.-L. Taberna, S. H. Tolbert, H. D. Abruña, P. Simon, and B. Dunn, "High-rate electrochemical energy storage through Li^+ intercalation pseudocapacitance," *Nature Mater.*, vol. 12, no. 6, pp. 518–522, Jun. 2013.
[37] S. Park, H. Park, S. Seong, and Y. Chung, "Multilayer substrate to use brittle materials in flexible electronics," *Sci. Rep.*, vol. 10, no. 1, pp. 1–8, May 2020.

[38] E. Bihar, T. Roberts, M. Saadaoui, T. Hervé, J. B. De Graaf, and G. G. Malliaras, "Inkjet-printed PEDOT: PSS electrodes on paper for electrocardiography," *Adv. Healthcare Mater.*, vol. 6, no. 6, Mar. 2017, Art. no. 1601167.
[39] R. R. Rajanna, N. Sriraam, P. R. Vittal, and U. Arun, "Performance evaluation of woven conductive dry textile electrodes for continuous ECG signals acquisition," *IEEE Sensors J.*, vol. 20, no. 3, pp. 1573–1581, Feb. 2020.
[40] S. Masihi, M. Panahi, D. Maddipatla, A. J. Hanson, S. Fenech, L. Bonek, N. Sapoznik, P. D. Fleming, B. J. Bazuin, and M. Z. Atashbar, "Development of a flexible wireless ECG monitoring device with dry fabric electrodes for wearable applications," *IEEE Sensors J.*, early access, Sep. 29, 2021, doi: 10.1109/JSEN.2021.3116215.
[41] J. Cui, S. B. Adeloju, and Y. Wu, "Integration of a highly ordered gold nanowires array with glucose oxidase for ultra-sensitive glucose detection," *Analytica Chim. Acta*, vol. 809, pp. 134–140, Jan. 2014.
[42] B. Z. Yu, Y. Moussy, and F. Moussy, "Coil-type implantable glucose biosensor with excess enzyme loading," *Frontiers Biosci.*, vol. 10, pp. 512–520, Jan. 2005.
[43] B. Yu, N. Long, Y. Moussy, and F. Moussy, "A long-term flexible minimally-invasive implantable glucose biosensor based on an epoxy-enhanced polyurethane membrane," *Biosensors Bioelectron.*, vol. 21, no. 12, pp. 2275–2282, Jun. 2006.
[44] A. Müsse, F. La Malfa, V. Brunetti, F. Rizzi, and M. De Vittorio, "Flexible enzymatic glucose electrochemical sensor based on polystyrene-gold electrodes," *Micromachines*, vol. 12, no. 7, p. 805, Jul. 2021.
[45] X. Xiao, J. Ulstrup, H. Li, M. Wang, J. Zhang, and P. Si, "Nanoporous gold assembly of glucose oxidase for electrochemical biosensing," *Electrochimica Acta*, vol. 130, pp. 559–567, Jun. 2014.
[46] C. Wu, H. Sun, Y. Li, X. Liu, X. Du, X. Wang, and P. Xu, "Biosensor based on glucose oxidase-nanoporous gold co-catalysis for glucose detection," *Biosensors Bioelectron.*, vol. 66, pp. 350–355, Apr. 2015.
[47] X. Jin, G. Li, T. Xu, L. Su, D. Yan, and X. Zhang, "Fully integrated flexible biosensor for wearable continuous glucose monitoring," *Biosensors Bioelectron.*, vol. 196, Jan. 2022, Art. no. 113760.
[48] D. U. J. Jung, R. Ahmad, and Y. B. Hahn, "Nonenzymatic flexible field-effect transistor based glucose sensor fabricated using NiO quantum dots modified ZnO nanorods," *J. Colloid Interface Sci.*, vol. 512, pp. 21–28, Feb. 2018.

JINPYEO JEUNG received the B.S. degree in electrical engineering from the Pohang University of Science and Technology (POSTECH), South Korea, in 2018, where he is currently pursuing the Ph.D. degree. He studies flexible device fabrication for wearable healthcare applications and electrode characterizations.

INYEOL YUN (Student Member, IEEE) received the B.S. and M.S. degrees in electrical engineering from POSTECH, in 2016 and 2018, respectively, where he is currently pursuing the Ph.D. degree. His research interest includes wearable healthcare devices.

YUNSIK KIM received the B.S. degree in electrical engineering from POSTECH, in 2021, where he is currently pursuing the Ph.D. degree. He studies wearable healthcare device and its applications.

SUWON SEONG received the B.S. degree in electrical and computer engineering from the University of Seoul, in 2020, and the M.S. degree in electronic engineering from POSTECH, in 2021, where he is currently pursuing the Ph.D. degree. His research interest includes oxide semiconductor thin-film transistors for large-area applications.

YOONYOUNG CHUNG (Member, IEEE) received the B.S. degree in electrical engineering from POSTECH, in 2006, and the Ph.D. degree in electrical engineering from Stanford University, Stanford, CA, in 2012. From 2012 to 2014, he was a Research Fellow with the Polymer Research Institute, POSTECH, where he has been an Assistant Professor with the Department of Electrical Engineering, since 2015. His current research interests include flexible electronic devices for large-area/healthcare sensors and display applications.